Journal of Hydrology 612 (2022) 128021

Contents lists available at ScienceDirect

Journal of Hydrology

journal homepage: www.elsevier.com/locate/jhydrol

Research papers

Optimal management of mixed hydraulic barriers in coastal aquifers using multi-objective Bayesian optimization

Samia Saad [a,b,*], Akbar A. Javadi [c], Tinkle Chugh [d], Raziyeh Farmani [e]

[a] Department of Engineering, University of Exeter, Exeter, UK
[b] Department of Irrigation & Hydraulics, Ain Shams University, Cairo, Egypt
[c] Professor of Geotechnical Engineering, Department of Engineering, University of Exeter, Exeter, UK
[d] Department of Computer Science, University of Exeter, Exeter, UK
[e] Department of Engineering, University of Exeter, Exeter, UK

ARTICLE INFO

This manuscript was handled by C. Corradini, Editor-in-Chief, with the assistance of Dongmei Han, Associate Editor

Keywords:
Seawater intrusion
Coastal aquifer management
Gaussian processes
Surrogate model
Hydraulic barriers
Computationally expensive

ABSTRACT

Mixed hydraulic barriers is an effective method to control seawater intrusion (SWI), particularly in regions that suffer from water shortages. However, determining the optimal well locations and rates for injection and abstraction is challenging due to the computational burden resulting from the huge number of calls for the high-fidelity hydrogeological simulation model. To alleviate this issue, we utilized a constrained multi-objective Bayesian optimization (BO) approach to optimize rates and locations of the hydraulic barriers to minimize total cost, aquifer salinity, and salt-wedge intrusion length, while satisfying regional abstractions with acceptable salinity levels. BO is useful for optimizing computationally expensive problems in few iterations by using a surrogate model and an acquisition function. Despite being an efficient optimization tool, the use of BO in the field of coastal aquifer management has not been explored. The proposed framework was evaluated on an unconfined aquifer subjected to three management scenarios considering different physical and technical constraints and was benchmarked against the widely used robust NSGA-II (Non-dominated Sorting Genetic Algorithm II) method. The results proved the effectiveness of BO in achieving an optimum mixed hydraulic barriers design in much fewer runs of the variable density aquifer model. BO with 350 evaluations yielded comparable results to 4150 evaluations using NSGA-II. BO solutions were spatially well-distributed along the approximated Pareto front. For the same number of evaluations, the hypervolume obtained by BO was larger by 30%. Based on different scenarios, the average amount of water required for abstraction ranged from 1.5% to 25% of that for injection. The injection has a significant impact on SWI management, but the abstracted water provides an alternative source of water. A sensitivity analysis was conducted on the optimization problem to illustrate its efficiency by omitting the barriers one at a time and assessing impacts on objective and constraint functions.

1. Introduction

Groundwater is an essential source of freshwater, accounting for about 30.1% of the world's available freshwater (Herrera-Franco et al., 2022). Given its relatively stable yield of high-quality water, groundwater has emerged as a vital water resource to meet domestic, industrial, agricultural, and environmental demands (Howard, 2015). Although groundwater is often relatively well protected from pollution, poor management has resulted in negative impacts such as declining aquifer heads, groundwater quality deterioration, lower yields, land subsidence, and, more notably, seawater intrusion (Bachtouli and Comte, 2019; Van Ty et al., 2021).

The literature shows that intensive research has been carried out on how to control SWI in aquifers. Implementing a mixed hydraulic barrier remediation system, a combination of negative and positive barriers, was proved to be more efficient than single barrier systems in controlling SWI (Ebeling et al., 2019; Shi et al., 2020). However, given the complexity of the mixed barrier systems, the design of such a system called for evaluating several design parameters, including pumping flow rates and positioning abstraction/injection wells within an aquifer.

Generally, the optimum configuration and rates are found by applying a numerical model that captures the groundwater flow pattern

* Corresponding author at: Department of Engineering, University of Exeter, Exeter, UK.
E-mail address: ss936@exeter.ac.uk (S. Saad).

https://doi.org/10.1016/j.jhydrol.2022.128021
Received 20 November 2021; Received in revised form 28 May 2022; Accepted 2 June 2022
Available online 11 June 2022

in the area followed by an optimization technique to achieve the best design for a system of wells. However, building a variable density-dependent groundwater flow and mass transport simulation model is computationally expensive (Asher et al., 2015). Alternatively, recent research studies shifted into using a surrogate model to replace the high-fidelity simulation model. Surrogate models have proven to be able to capture the dynamic behavior of SWI at a significantly less computational cost (Kopsiaftis et al., 2019; Rajabi and Ketabchi, 2017; Roy and Datta, 2020). A surrogate model can be defined as a "model of the model," where it is a statistical data-driven model describing the relationship between model adjustable parameters (inputs) and the response surface of the simulation model (outputs) (Wang et al., 2014). Many response surface approximation techniques have been utilized as surrogate models to replace the high-fidelity groundwater simulation models (Artificial Neural Network (ANN), Gaussian process regression (GPR), Radial basis function (RBF), polynomials, etc.). Although no approximation technique performs best universally, and the results rely on many factors, such as its structure, parameters, size of the training set, and data sampling method, there is a general agreement on the strength of GPR, also known as Kriging, and RBF based optimization frameworks (Asher et al., 2015; Jones et al., 1998; Razavi et al., 2012). The GPR model parameters are learned in a Bayesian scheme, thus predicting unobserved inputs needs to integrate over all parameter values weighted by their probability distribution, given the training data. Accordingly, GPR can estimate the uncertainty in the predictions of the surrogate model (Rasmussen and Williams, 2006). It considers the deterministic response of the simulation model as a realization of a stochastic process (Razavi et al., 2012).

Few studies have used GPR as a data-driven surrogate model in SWI management. For example, Rajabi and Ketabchi (2017) used GPR as a surrogate model to replace the 3D density-dependent SUTRA simulation model. The trained GPR model was coupled with Monte Carlo simulation to generate probability distributions of salinity concentrations in the observation wells. These probability distributions were passed to the Continuous ant colony optimization algorithm to optimize the extraction rates in the wells under constraints related to SWI extent. Kopsiaftis et al. (2019) investigated the capacity of substituting the GPR as a surrogate model for variable density models to predict the SWI extent. The study compared the obtained results with other methods. The results proved that GPR was more efficient in terms of different statistical indicators, however, it was more time-consuming.

Bayesian optimization (BO) can provide optimum solutions using the least number of expensive evaluations (Jones et al., 1998; Yang et al., 2019b). This feature makes BO a powerful tool for solving design problems in a wide range of fields (Shahriari et al., 2016). Additionally, it has emerged as a Green Artificial intelligence approach. It can save the energy consumed for training and validating, hence reducing the emission of carbon dioxide (Candelieri et al., 2021). BO addresses the problem of searching for the global optimum by learning from the previous evaluations to suggest the next promising point to sample (Jones et al., 1998). All available information on the objective functions that can be provided before evaluating them at any sampling point is specified through a prior probability distribution. A probabilistic model (e.g., GPR) sets this prior distribution over the optimization function, which is conditioned using previous evaluations to provide a posterior distribution. The posterior is updated iteratively by the latest sampled function evaluation to represent our updated belief on the function given the observed data. BO uses the probabilistic surrogate models to design an acquisition function. The acquisition function is a preselection computationally inexpensive function that can be evaluated at a given point to estimate the improvement in the performance considering the uncertainty in the posterior. Thus, on its optimization, it can guide to the new input location in which the objective functions should be evaluated in each iteration.

BO has been applied in some groundwater modeling applications. For example, Pirot et al. (2019) applied the BO to identify the contaminant source characteristics in an aquifer with a high degree of heterogeneity, and different connectivity patterns. The study aimed to minimize an objective function that describes the temporally variable misfit between observed and simulated contaminant levels at 25 monitoring wells. A significant decrease in the required number of function evaluations for convergence was observed at 50 evaluations instead of more than 2600 that would have been needed to perform an exhaustive evaluation of points over the discrete domain. Krityakierne and Baowan (2020) proposed an aggregate Gaussian process (GP) model with an expected improvement criterion to construct a simulation-based optimization algorithm to identify the location of the contaminant source. An aggregated GP model approximates the exact GP model, which enables the handling of many input data points. Pourmohamad and Lee (2021) presented a BO approach that links GPR surrogate modeling with barrier functions to solve the problem of controlling the migration of two plumes of chlorinated contaminants with the minimization of the pump and treat remediation cost. They used the barrier functions aiming to reduce the objective function while satisfying the constraint space. Despite these studies, limited information is established in the literature regarding the implementation of BO to solve multi-objective optimization problems in groundwater applications.

A multi-objective optimization problem is a challenge of maximizing/minimizing the utility values of multiple, typically conflicting, objective functions simultaneously. The goal is to identify the set of Pareto optimal solutions, in which any improvement in one objective causes deterioration to another. The hypervolume measure indicates the size of the dominated region of the objective space by the Pareto optimal set. It is widely used in designing and assessing the performance of multi-objective optimization techniques (Li and Yao, 2019). In the context of BO, Emmerich et al. (2006) proposed the expected hypervolume improvement (EHVI) as a measurement of the hypervolume improvement resulting from evaluating a new candidate point, taking into consideration the uncertainty of the prediction. EHVI has been a commonly used criterion, whereby in comparison to other criteria, it achieves good convergence and diversity to a true Pareto front (Luo et al., 2014; Yang et al., 2019a), and yields excellent results when applied as an acquisition function in BO studies (Balandat et al., 2020; Yang et al., 2019b). However, its calculation was criticized for its high computational complexity (Daulton et al., 2020; Yang et al., 2019b). To calculate it, the first method was suggested by Emmerich et al. (2006) using Monte Carlo (MC) integration method. Efficient EHVI computation has been the subject of a large body of research e.g. (Emmerich et al., 2011; Hupkens et al., 2015; Yang et al., 2019a; Yang et al., 2019b). Recently, a batch version of EHVI called q-Expected Hypervolume Improvement (qEHVI) was proposed in Daulton et al. (2020) study. The qEHVI provides the closed-form of EHVI with Monte Carlo (MC) approximation and can handle q points in parallel (Daulton et al., 2020). Specifically, qEHVI enhances the efficiency of the computations by calculating the exact gradients of the MC estimator using the auto-differentiation method and then optimizing EHVI using the gradient information.

This study aims to 1) introduce the application of BO in solving SWI management problems, and 2) evaluate its performance against the NSGA-II optimization approach, which is considered a robust multi-objective optimizer, yet well known for its requirement of many function evaluations (Deb et al., 2002), and 3) test its robustness on different management scenarios to obtain the optimum locations and rates for the mixed hydraulic barriers through a constrained multi-objective methodology. The methodology involves minimization of the average intrusion length, the total salt mass within the aquifer, and the total cost subject to the supply of the required demand with permissible salinity concentration. The optimization algorithm is based on GPR and the qEHVI. The developed management model will be applied to an aquifer that is threatened by lateral seawater intrusion due to overexploitation. The model incorporates 3D density-dependent miscible flow and transport of seawater.

2. Methodology

2.1. Density-dependent flow and transport simulation model

A three-dimensional transient density-dependent flow and mass transport finite element model was developed using FEFLOW software (Diersch, 1988) and used to simulate the SWI in a coastal aquifer under the influence of regional pumping. In the present study, the porous medium is considered fully saturated. Oberbeck-Boussinesq approximation for the nonlinearity in the fluid density is used (Boussinesq, 1903), where density variations induced by variations in solute concentration are all neglected except for the buoyancy term in the momentum equation. The viscosity is considered to be independent of the concentration, and thermal effects are neglected.

The governing equations of coupled groundwater flow and salt mass transport describing the seawater intrusion phenomenon can be found in detailed descriptions on Diersch (2013).

2.2. Design of experiments (DoE)

Latin Hypercube and Quasi-Monte Carlo are commonly used in surrogate modeling-based optimization as a space-filling design due to their flexible sample sizes, good distribution on the whole space with a relatively small number of sample points (Wang et al., 2014). In this work, Latin Hypercube sampling (LHS) and conditioned Latin Hypercube sampling (cLHS) methods are employed. The former method was used to generate different realizations for abstraction/injection rates, while the latter was utilized for the spatial coordinates sampling at a selected number of abstraction and injection barrier wells.

LHS is a stratified random procedure that generates sampling variables from their multidimensional distributions. It provides full coverage of each variable range by dividing it into a number of strata equal to the sample size, and the probability of the sample falling in each stratum is one over the sample size (McKay et al., 1979).

The cLHS is a sampling strategy of an area with prior information expressed as ancillary data. The search algorithm aims to select optimal sampling locations through the ancillary data while obtaining a Latin hypercube of the variables' distributions (Minasny and McBratney, 2006). Normally, the aquifer domain has an irregular spatial boundary or has some locations that need to be excluded from the sampling selection due to either their subsurface geological formations (i.e, ophiolite) or the land cover occupied by water bodies, buildings, roads, etc. These considerations can be taken into account using cLHS for spatial locations sampling. However, LHS stratifies each variable independently, which may result in combinations of the variables' values that are not related to any existing point in reality.

The training data set, $D = \{(X, Y, G) | X \in \Re^{(N\times d)}, Y \in \Re^{(N\times m)}, G \in \Re^{(N\times g)}\}$ of size N with d decision variables, m objective functions, and g constraint functions, defines the input–output pairs which are used to train the proposed surrogate model. Abstraction/Injection rates and spatial locations at a required number of hydraulic barrier wells are the inputs to the numerical simulation model and represent the decision variables. They were used to obtain the total salt mass within the aquifer, the average inland length of the saltwater wedge intrusion, measured from the coastline, and the salinity at each regional abstraction well. These simulation results in addition to the total cost of the management scenario and other environmental/physical constraints (described in Section 2.5) are considered as the outputs constituting the objective and constraint functions.

2.3. Surrogate assisted simulation–optimization model

In this study, a surrogate model-based optimization of abstraction/injection rates and well locations in mixed hydraulic barrier systems in coastal aquifers is performed. FEFLOW is integrated with the Bayesian optimization model using custom Python scripts for optimizing the proposed coastal management strategy. This coupling is done automatically in a dynamic manner as the Python script calls FEFLOW to pass the information back and forth for each iteration. The BO approach is implemented in BoTorch open-source library (Balandat et al., 2020).

2.3.1. Bayesian optimization

Bayesian optimization is effective for optimizing functions that are time-consuming to evaluate, lack an analytical expression, and are subject to noise in their evaluations (Jones et al., 1998). Such objective functions without analytical formulations are black-box functions (Garrido-Merchán and Hernández-Lobato, 2020). In this work, the objective and constraint functions f, in which their values are obtained by calling the FEFLOW simulator, are black-box. BO is then used to find the optimal design variables.

The BO algorithm is an adaptive sequential design algorithm. It consists of two iterative operations: 1) building probabilistic models on the training dataset (D) that substitute the high fidelity numerical simulation model to describe the objectives and constraint functions. In this work, GPR models (described in Section 2.3.2) are built for each function. 2) finding new promising sample(s) (or decision vectors) by using these models to optimize the acquisition function (also known as an infill criterion). In this work, we use the qEHVI with the probability of feasibility (to handle constraints) as the acquisition function (described in Section 2.3.3).

The new promising sample(s) are re-evaluated with the expensive functions by calling the simulation model. The new data is then appended to the existing training dataset and GPR models are re-trained. This process is continued until a termination criterion (usually a maximum number of expensive evaluations) is met. The non-dominated solutions from all expensive evaluations are then used as the final solutions. A flow chart of the surrogate-assisted simulation–optimization model using Bayesian optimization with Gaussian Process framework is presented in Fig. 1.

2.3.2. Gaussian process regression

GPR is a distribution for each black-box function f, where $f(x)$ of each point x has a prior multivariate normal distribution, and any finite number of these random points x has a joint Gaussian distribution, thereby GPR is a collection of functions (O'Hagan, 2006; Rasmussen and Williams, 2006). This distribution is defined by the mean function (that describes the approximated function trend) and the covariance function (that describes the prior belief of the unknown function that needs to be modeled such as its smoothness, amplitude, etc). A GPR defines a prior over an infinite number of functions that are defined by the covariance function. Given the observed data of the training dataset (D), it is converted to a posterior distribution $p(f|D)$ over possible functions that fit the observed data, it reflects the uncertainty in the model estimations arising from the choice of the design parameters that define the model. The observed data restrict the joint distribution to contain only those functions which agree with the observations (Rasmussen and Williams, 2006). Providing such predictive distribution is explicitly available in some function approximation techniques, (e.g., in polynomials, GPR, Random Forests, and Gaussian radial basis function models) (Razavi et al., 2012). GPR is chosen in this study for the following reasons:

(1) It is a probabilistic approach, and can estimate the uncertainty in the prediction (Rasmussen and Williams, 2006), which makes them more useful than other regression methods such as Neural networks. (2) It is a non-parametric model and doesn't depend on user-specified parameters e.g. number of hidden layers and nodes in the neural network. A GPR model can be fully specified by mean and covariance functions, which leads to a simple structure (described below) (O'Hagan, 2006; Rasmussen and Williams, 2006). (3) It is analytically tractable (O'Hagan, 2006; Rasmussen and Williams, 2006). (4) It can incorporate prior knowledge of the outputs in the surrogate construction process (O'Hagan, 2006; Rasmussen and Williams, 2006). (5) It has shown its potential

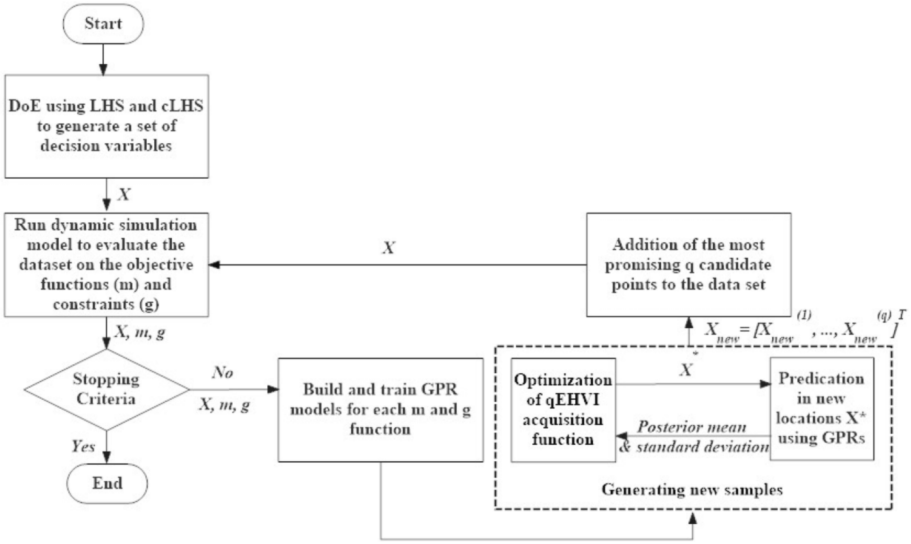

Fig. 1. Steps of the BO approach.

in capturing SWI behavior with high accuracy (Kopsiaftis et al., 2019; Lal and Datta, 2020; Rajabi and Ketabchi, 2017).

For each objective function and constraint function, we build a GPR model. Let us denote the function values for the i^{th} objective function or constraint function with y. A GP is then a multivariate normal distribution:

$$y = \mathcal{N}(\mu, K) \tag{1}$$

where μ is the mean and K is the covariance matrix The mean function is unknown priorly but is assumed as constant in this study. The covariance matrix K measures the correlations between different points in the data set. The covariance matrix relies on the covariance function (or kernel function), which provides a pair-wise correlation between two data points in the data set. There are many covariance functions used in the GPR e.g. Gaussian kernel (also known as radial basis function kernel and squared exponential kernel), Matern kernel, and periodic kernel. This work used the Matern 5/2 covariance function, which is recommended for modeling realistic functions (Snoek et al., 2012). It depends solely on the Euclidean distance between observations made at two decision vectors. Training of the GPR model incorporates finding the optimal values of the design parameters (hyperparameters) upon which the covariance functions depend to allow a better fit of the data. The hyperparameters vector includes the amplitude, length scales, and the standard deviation of the noise in the observations. For more details on these parameters and their significance, refer to Rasmussen and Williams (2006). The log marginal likelihood function is maximized to estimate these parameters (see Rasmussen and Williams (2006)). This completes the building of a GPR model. This model is then used to get the posterior distribution (i.e. approximations and their uncertainty). In GPR, the posterior distribution is also Gaussian. For a new set X^*, the posterior distribution is given by:

$$p(y^*|X^*, X, y, \Theta) = \mathcal{N}\left(K(X^*, X)\left[K(X, X) + {\sigma_n}^2 I\right]^{-1} y, K(X^*, X^*) - K(X^*, X)^T\left[K(X, X) + {\sigma_n}^2 I\right]^{-1} K(X, X^*)\right) \tag{2}$$

where, X, y are the matrics of input–output pairs forming the training data set, Θ is the estimated hyperparameters vector, σ_n is the standard deviation of the noise in the observations, I is the identity matrix, and K (.,.) represents the covariance matrix. In the equation above, $K(X^*, X)\left[K(X, X) + {\sigma_n}^2 I\right]^{-1} y$ are the posterior means (or point approximations), and $K(X^*, X^*) - K(X^*, X)^T\left[K(X, X) + {\sigma_n}^2 I\right]^{-1} K(X, X^*)$ is the covariance matrix representing the uncertainty in approximations. The uncertainty can be obtained by taking the square root of diagonal elements in this matrix. In this work, this posterior predictive distribution is used when maximizing the qEHVI to find promising decision vectors. Further information on the used Matern covariance function and the log marginal likelihood function can be found in supplementary data (S1).

2.3.3. Acquisition function: differentiable q-expected hypervolume improvement

Expected Hypervolume Improvement (EHVI) is based on the hypervolume indicator to indicate the quality of a solution set in multi-objective problems. The hypervolume is the only known strict Pareto compliance that measures both convergence and diversity among the set of nondominated solutions (Zitzler et al., 2007). It measures the size or hypervolume of the space dominated by a finite approximate Pareto set $\mathcal{P}$ and bounded below by a reference point r. r is chosen to satisfy the condition that all the solutions of the Pareto-front approximation sets, that might occur during the optimization process are to be dominated. EHVI needs to be evaluated many times in the process of searching for the optimal point based on the GPR models. The algorithm becomes computationally expensive to evaluate when it is not expressed in a closed form (analytical expression) (Daulton et al., 2020; Yang et al., 2019b). Additionally, the computational complexity is increased when it relies on gradient-free or approximated gradients for its optimization (Daulton et al., 2020). qEHVI, recently derived by Daulton et al. (2020) overcomes these limitations by providing the closed-form and computing the exact gradient of the Monte-Carlo (MC) estimator using auto-differentiation. Auto-differentiation makes using gradient-based optimization for complex acquisition functions and objectives straightforward. In addition, qEHVI provides the benefit of evaluating multiple samples (q) in parallel. Evaluating samples is important especially when parallel processing units or computers are available. Further details on qEHVI can be found in (Daulton et al., 2020) and the EHVI acquisition

function is described briefly in the supplementary data (S2). The constraints are introduced to the optimization by assuming them as black-box functions. The feasible Pareto set is identified as the Pareto set that satisfies g(x) ≤ 0 and the qEHVI acquisition function handles them through weighting the hypervolume improvement of the objective vectors by the probability of feasibility (0 and 1 for infeasible and feasible solutions respectively).

2.4. Direct simulation–optimization model

This work also used the NSGA-II (Deb et al., 2002) to solve the given multi-objective optimization problem through the direct simulation–optimization framework. NSGA- II is an elitist multi-objective evolutionary algorithm based on non dominated sorting approach. NSGA-II seeks Pareto-optimal solutions by directing nondominated solutions in a particular generation toward Pareto-optimal solutions while maintaining diversity among the solutions with the aid of the crowding distance. To handle the constraints in NSGA-II, we used the approach proposed in Deb et al. (2002).

The numerical simulation model was directly linked with the optimization model. The optimization search process was performed by iterating between FEFLOW simulation model and NSGA-II optimization model. Fig. 2 presents the developed methodology of NSGA- II.

2.5. Multi-objective optimization problem formulation and constraints

In the present work, the problem of optimization of wells locations and injection/abstraction rates of the proposed management model is considered as a non-linear multi-objective constrained optimization problem and is expressed as follows:

$$f_1 = maximize - \left(\int s\varepsilon C dV \right) \tag{3}$$

$$f_2 = \text{maximize} - \left(avg \sum_{i=1}^{n_c} l_{50} \right) \tag{4}$$

$$f_3 = maximize - \left(\sum_{i=1}^{N_w^{abs}} \xi_{abs} . |Q_i^{abs}| + \sum_{i=1}^{N_w^{Inj}} \xi_{Inj} . |Q_i^{Inj}| + \sum_{i=1}^{N_w} \xi_{construction} . D_i \right) \tag{5}$$

$$s.t, g_1 = C_i^{PW} \leq C_{UCL} \tag{6}$$

$$g_2 = \sum_{i=1}^{N_w^{abs}} Q_i^{abs} \leqslant Q^{abs} \tag{7}$$

$$g_3 = \sum_{i=1}^{N_w^{Inj}} Q_i^{inj} \leqslant Q_{\max}^{inj} \tag{8}$$

The negative sign in the objective function is because the goal of the management is to minimize, and the used library BoTorch assumes maximization. The decision variables take values in the d-dimensional continuous space $[\boldsymbol{l}, \boldsymbol{u}] \subset \mathbb{R}^{\boldsymbol{d}}$ in which they are treated as continuous variables rather than discrete ones. They are described as follows:

$$\boldsymbol{q_{min}} \leq \boldsymbol{q_i} \leq \boldsymbol{q_{max}}, \forall \boldsymbol{i} \in \{1, ..., \boldsymbol{N_w}\}$$

$$\boldsymbol{x_{min}} \leq \boldsymbol{x_i} \leq \boldsymbol{x_{max}}, \forall \boldsymbol{i} \in \{1, ..., \boldsymbol{N_w}\}$$

$$\boldsymbol{y_{min}} \leq \boldsymbol{y_i} \leq \boldsymbol{y_{max}}, \forall \boldsymbol{i} \in \{1, ..., \boldsymbol{N_w}\} \tag{9}$$

In the above equations; $\int \boldsymbol{s\varepsilon C dV}$ is the total salt mass within the aquifer domain (g), where $\int \boldsymbol{s\varepsilon dV}$ is the fluid volume (m^3), s is the fluid saturation ratio; it equals 1 in fully saturated porous media, $\boldsymbol{\varepsilon}$ is the porosity, and $\boldsymbol{C}$ is the solute concentration per fluid volume (g/m^3). $\boldsymbol{l_{50}}$ is the 50% isochlor intrusion length, measured per each node that lies on the coastline (m). $\boldsymbol{n_c}$ is the number of nodes that lie on the coastline. $\boldsymbol{N_w} = \boldsymbol{N_w^{abs}} + \boldsymbol{N_w^{Inj}}$, $\boldsymbol{N_w^{abs}}, \boldsymbol{N_w^{Inj}}$ are the numbers of abstraction and injection

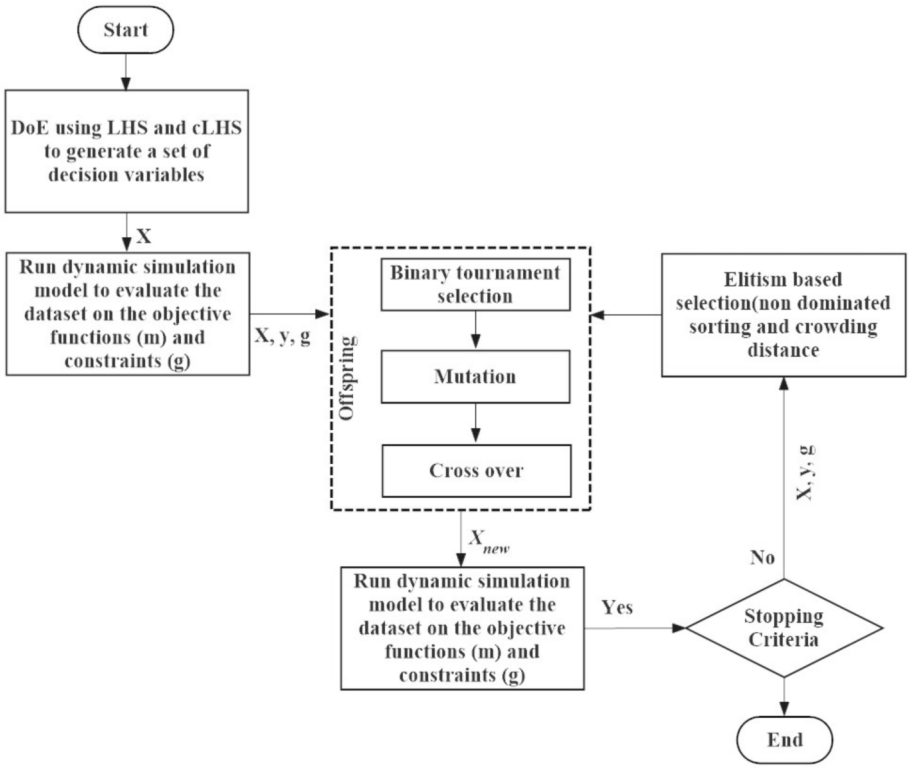

Fig. 2. Steps of NSGA-II algorithm.

wells of the hydraulic barrier system, respectively. ξ_{abs}, ξ_{Inj} are the operational costs of abstraction and injection per unit flow respectively (£ /m^3/day), £ represents a monetary unit. Q_i^{abs}, Q_i^{Inj} are the abstraction and injection rates (m^3/day). $\xi_{construction}$ is the construction cost of a well per unit depth (£/m). D_i is the depth of a well (m). C_i^{PW} is the concentration of water pumped from the regional pumping wells (PW) (g/m^3). Q^{abs} is the amount of abstracted water by the hydraulic barriers either to be disposed of (positive sign) or required to be used (negative sign) (m^3/day). Q_{max}^{Inj} is the maximum amount of injected water (m^3/day). q_i is the abstraction/injection rate at i^{th} hydraulic barrier well; the rates are positive in the case of the negative barrier, and negative in the case of the positive barrier (m^3/day). x_i, y_i are the × and y coordinates of i^{th} hydraulic barrier well (m).

The imposed environmental constraints are to ensure that the salinity at the regional abstraction wells, the total amounts of injection of positive hydraulic barriers, the total amounts of abstraction from negative hydraulic barriers, and either abstraction or recharge rate per each barrier are within the permissible limits.

2.6. Coastal aquifer management scenarios

For each management scenario, the remediation management started, when the salinity concentration of the pumped water at any regional pumping well exceeded the upper concentration limit (C_{UCL}). In this study, the upper concentration limit (C_{UCL}) is considered 1000 mg/l to comply with the acceptable limit for total dissolved salts in the drinking water and irrigation uses (Ayers et al., 1985; World Health Organization, 2004).

The optimization problems of three different management scenarios were solved to 1) test the robustness and performance of the Bayesian optimization approach, and 2) formulate some of the realistic physical and environmental site-specific conditions.

Management scenario 1: Full supply for regional abstractions was maintained,

Management scenario 2: Regional abstractions stopped,

Management scenario 3: Constraints were imposed on the allowable locations for abstraction hydraulic barriers, and the minimum volume to be abstracted by them to feed a desalination plant, in addition to the full supply for the current regional abstractions.

The rates and locations of the injection/abstraction hydraulic barriers were optimized to achieve the management objectives, subject to the above-mentioned constraints for management scenarios 1 and 2. However, for management scenario 3, a constraint was added to force the abstraction barriers to be located near the initial toe location along the aquifer width or further seaward. The goals of management scenario 3 were to supply freshwater to the regional abstractions, supply brackish water to feed the desalination plant, and mitigate the SWI. This scenario addresses the problem of satisfying conflicting requirements such as SWI management, desalination of brackish water, and aquaculture industry, which was recorded in different aquifers e.g. (Park and Shi, 2015). Moreover, site requirements may impose constraints on the potential locations for the hydraulic barriers in advance. Accordingly, this constraint is added to test the robustness of the BO algorithm for handling this constraint.

$$g_4 = \frac{1}{x_{toe}} \sum_{i=1}^{N_w^{abs}} \max(-x_i + x_{toe}, 0) \quad (10)$$

x_{toe} is the initial toe coordinate in the X-direction (m).

3. Evaluation of the proposed methodology on a case study

Our goals were to examine the effectiveness of using the BO approach in the convergence towards the approximated Pareto front under a restricted computational effort in the coastal management problems and to compare the performance of BO against NSGA-II. However, the NSGA-II model was run under a very large of simulations (4000 simulations), in order for its results to be used as a baseline. The relatively short simulation time compared to the real-world problems makes the illustrative case study suitable for the current study. The computational time required for one run using the numerical simulation model is approximately 7 min on a desktop PC with a 3.4 GHz Intel i5 processor and 8 GB of RAM. The assumption of imposing strong restrictions on the possible number of simulations using a high fidelity model in real-world coastal aquifer management problems is more realistic and practical (Christelis et al., 2018).

The aquifer considered is an unconfined, anisotropic, homogenous, shallow coastal aquifer. The model boundary has a rectangular shape. The horizontal dimensions are × = 5000 m, y = 2500 m, and the vertical dimension is z = -25 m below the sea level, where the aquifer base is located. The regional abstractions are supplied by 8 fully penetrating pumping wells placed between 1000 and 3000 m from the shoreline representing the regional pumping field with a total water demand of 4000 m^3/day equally distributed among them. The injected water of the positive hydraulic barriers, to recharge the aquifer, is considered the effluent of tertiary treated wastewater, and its salinity is considered 500 mg/l (Metcalf et al., 2014). The spatial and temporal discretizations of the numerical model are further discussed in the supplementary data (S3). The management period is considered 10 years (Ebeling et al., 2019); i.e. all the objectives' and constraints' values were determined at the end of this period. Table 1 shows the considered hydrogeological parameters in the simulation model.

The 3D view of the coastal aquifer model with the imposed flow and transport boundary conditions, the initial hydraulic head, and salinity distributions, just before the management started are presented in Fig. 3.

The number of decision variables is 18 corresponding to the rates, x and y coordinates of 6 (N_w) potential fully penetrating hydraulic barriers. The lower and upper permissible limits for the rates and coordinates variable of each hydraulic barrier for the management scenarios are shown in Table 2 and further discussed in the supplementary material (S4). The potential locations for the barriers were selected from the shoreline to 1930 m inland horizontally (in the x-axis direction) and along the whole aquifer in the y-axis direction to accommodate the saline wedge and extend into the regional pumping field. The imposed constraints for each management scenario are shown in Table 2. The average initial × coordinate of the toe is 4215 m. The cost coefficients were assumed, for the sake of simplicity, to be equal to the unity ($\xi_{abs}, \xi_{Inj} and \xi_{construction}$), however, in reality, they have to be estimated using more complex formulae.

The reference point (r) is taken in this work as [-2.2*10^{11} g, −500 m, -£ 8000] for the three objectives; total mass of salt, the average intrusion length of 50%, and the total cost respectively, which are considered as the minimum acceptable value for each objective.

An initial DoE of size 150 is considered and 200 points are added in the BO process (100 iterations and q = 2). Therefore, the total number of expensive function evaluations was 350 in BO. The model runs were

Table 1
Aquifer parameters.

Parameter	Units	Value
Hydraulic conductivity in X-direction (K_x)	m/d	30
Hydraulic conductivity in Y-direction (K_y)	m/d	30
Anisotropy ratio(K_z/ K_x)	–	10
Molecular diffusion coefficient (D_d)	m^2/s	1×10^{-9}
Longitudianl dispersivity (β_l)	m	65
Transverse dispersivity (β_T)	m	6.5
Porosity (ε)	–	0.3
Specific yield	–	0.15
Fluid dynamic viscosity (μ_0)	kg/m.s	0.0011
Freshwater density (ρ_0)	kg/m^3	1000
Seawater density (ρ_s)	kg/m^3	1025

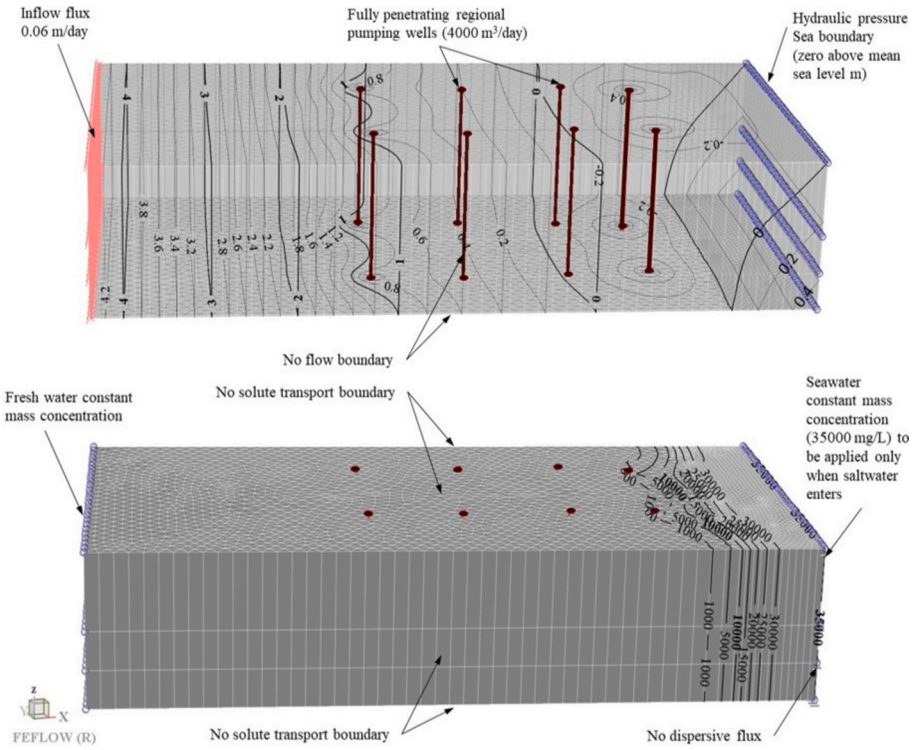

Fig. 3. 3D coastal aquifer model with applied initial and boundary conditions before the application of management strategy.

Table 2
Decision variables lower and upper bounds and the imposed constraints limits for each management scenario.

Scenario no.	Total no of hydraulic barriers N_w	Decision variables bounds			Constraints limit			
		X-coordinate (m)	Y-coordinate (m)	Rates per a barrier (m^3/day)	Salinity at regional pumping wells (mg/lit)	Amount of water injected by the barriers (m^3/day)	Amount of water abstracted by the barriers (m^3/day)	Negative hydraulic barriers X-coordinate (m)
Scenario1	6	3070 to 5000	0 to 2500	−1500 to + 1500	≤1000	≤ 8000	≤ 8000	–
Scenario2	6	3070 to 5000	0 to 2500	−500 to + 500	≤1000	≤ 8000	≤ 8000	–
Scenario3	6	3070 to 5000	0 to 2500	−1500 to + 1500	≤1000	≤ 8000	≥ 1000	4215 to 5000

parallelized over two cores of the used machine (four cores). Parallelization can achieve enhanced performance and faster convergence (Daulton et al., 2020).

The control parameters of NSGA-II algorithm were selected as initial training sample size 150, population size 20, the maximum number of generations 200, crossover probability 0.8, and mutation probability (1/ No. of decision variables) 0.056. For a fair comparison, the initial population generation for NSGA-II was set the training dataset of DoE. The total number of expensive function evaluations was 4150 in NSGA-II.

4. Results

This section is composed of three subsections. In Section 4.1. the performance of the BO approach was explored and compared against NSGA-II to investigate the quality of the solutions obtained by the BO approach in management scenario 1. In Section 4.2, the Pareto optimal front resulted from the optimal locations and rates of the mixed hydraulic barriers for the three management scenarios introduced in Section 2.6 were presented. Finally, in Section 4.3 the effectiveness of the optimal mixed hydraulic barrier remediation system in mitigating the SWI was evaluated for a randomly selected Pareto solution for management scenario 1 and compared to the natural intrusion condition. Furthermore, the efficiency of the optimization process is assessed by the omission of each of the hydraulic barriers successively from the system and testing its impact on the objective and constraint functions.

4.1. Bayesian optimization and NSGA-II

The optimization problem of management scenario 1 using the proposed approaches of BO and NSGA-II was solved. The optimal well locations and optimal rates for the mixed hydraulic barriers remediation system were obtained.

To investigate the quality of the obtained solutions by both approaches, the Pareto fronts of the feasible solutions (solutions that satisfy the constraints) are plotted for the BO and NSGA-II models in Fig. 4. The conflicting nature between the third objective (total cost) and either the first objective (total salt mass) or the second objective (the average intrusion length of 50%) can be concluded from the plots. The first and second objectives were not in conflict with each other. They were adopted to ensure that the management strategy is capable of the toe repulsion, as well as mitigating the risk of increasing the total aquifer salinity due to trapping the salt landside at the end of the management period. Hence, placing the positive barrier within the saltwater wedge may pose the potential of landside salt trapping (Ebeling et al., 2019),

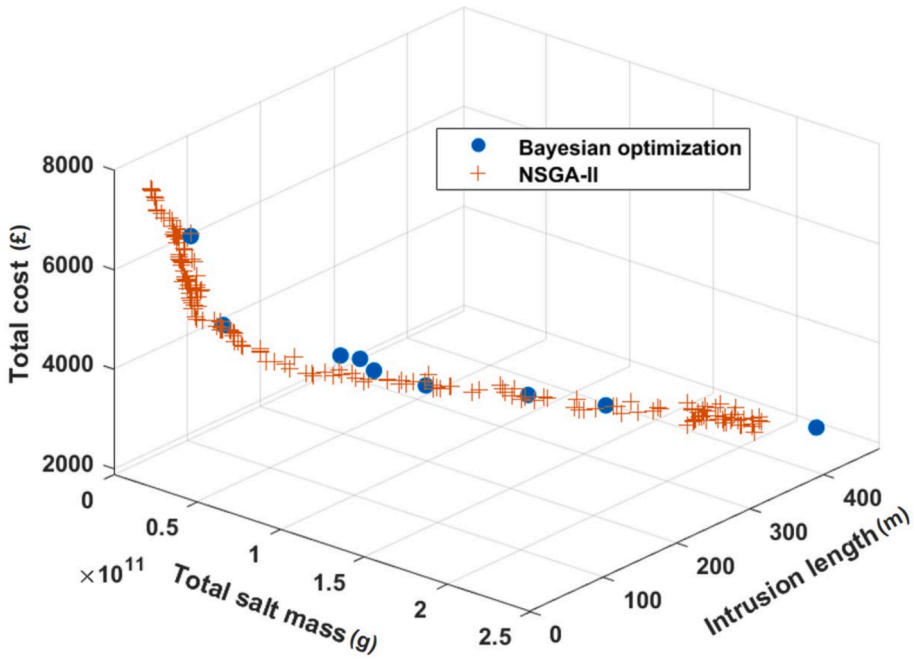

Fig. 4. Approximated Pareto fronts of management scenario 1 using BO & NSGA-II.

moreover, the salinity of the water used for injection may exaggerate this potential of salt trapping.

In Fig. 4, the BO approach succeeded to identify solutions on the Pareto front in an exceptionally low number of function evaluations. Moreover, the solutions with BO were well distributed along the approximated Pareto front. To evaluate the performance of BO against NSGA-II quantitively, three data analysis methods were used; 1) calculating the hypervolume (HV) and Generational distance (GD) which are the performance indicators for measuring convergence and diversity, and for measuring how the current non-dominated solutions are near to the optimal Pareto front respectively, 2) performing the one-way analysis of variance (ANOVA) test which provides evidence if there is a relationship between the means of the two Pareto solution sets, and 3) comparing between the data distribution of each approach by focusing on the spread.

A plot of HV with the number of expensive evaluations (or simulations) is shown in Fig. 5a. As can be seen, despite NSGA-II initially performing better than BO, at a few learning cycles BO took the lead. At the end of the BO optimization process of 350 evaluations (150 initial training data set + 100 × 2 iterations), the BO obtained better hypervolume, which shows an increase of about 30% compared to NSGA-II. For a similar hypervolume, the BO used 200 function evaluations, which is very low compared to 2400 evaluations by NSGA-II. GD is based on calculating the sum of adjacent distances of solution sets obtained by each approach to the reference points (Liu et al., 2019). The reference points represent the optimal Pareto front, which is not known a priori, therefore all solutions attained by the two approaches were considered to find non-dominated solutions. These solutions were used as reference points for GD calculations (Song et al., 2018). BO can efficiently improve the solutions without sacrificing the accuracy of Pareto optimal solutions while maintaining good convergence and diversity, as shown by its high HV and minimum GD values (Fig. 5b).

ANOVA test was executed for the solutions on the Pareto optimal objective functions sets and the p-value was calculated using ScipPy library. The smaller the p-value, the more the null hypothesis is considered not likely to be true and is significant to reject. Our null hypothesis is that the sample (BO approach results) was derived from the parent population (NSGA-II approach). In Fisher's approach, the threshold p-value is considered 0.05 (Fisher, 1992). The calculated p-values for the three objectives were 0.37, 0.43, and 0.34 respectively. The p-values are greater than 0.05, which illustrates that it is not statistically significant to reject the null hypothesis and there is convincing evidence to retain it.

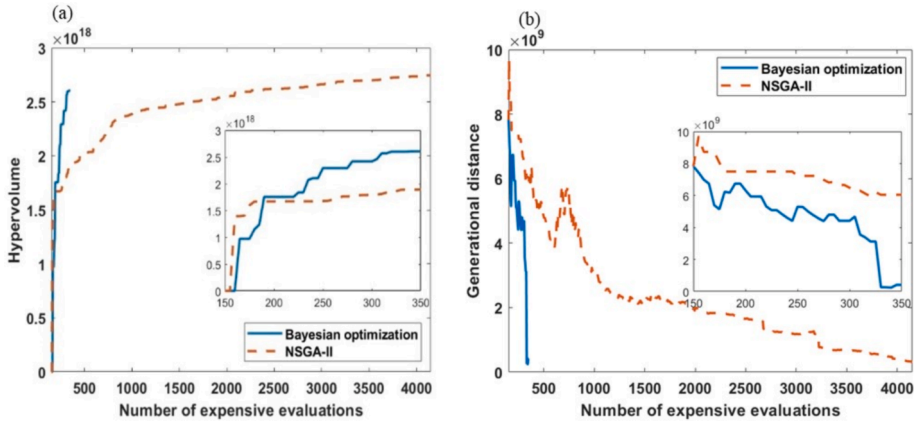

Fig. 5. Hypervolume and generational distance with number of expensive evaluations with BO and NSGA-II.

The third data analysis was to explore the spread out of the BO feasible solutions on the approximated Pareto front of the three objective functions relative to the NSGA-II approach. The ranges of the objectives that were obtained by NSGA-II were from 22 to 205 tons for the total salt mass, 0 to 433 m for the average intrusion length, and £2187 to £7880 for the total cost. Similarly, the ranges obtained by BO were 46 to 212 tons, 0 to 477 m, and £1879 to £7372 for the three objectives. The analysis revealed that even though the number of solutions that were obtained by the BO approach was less than that in the NSGA-II approach (Fig. 4), the BO solutions could cover approximately the entire range of each objective.

The main purpose of using a surrogate model in conjunction with BO is to quickly converge to an approximate region of Pareto-optimal solutions, allowing the needed computational time to be drastically reduced. The NSGA-II took about 371 h for 4000 evaluations and BO took only 19.34 h for 2×100 evaluations (parallel computing) to obtain approximately similar solutions and thus showing the efficiency and potential of BO in solving computationally expensive optimization problems. However, on the other side, more computations were considered by BO for one iteration. BO took around double the time, invested by NSGA-II. Table 3 shows the comparison between BO and NSGA-II approaches in terms of the computational time, performance indicators, and the range of objectives' values obtained by the Pareto solution sets.

Both approaches, NSGA-II and BO, were able to find feasible solutions near the approximated Pareto front. The main advantage of BO is that it found feasible solutions in a very low number of function evaluations. The search behavior of both approaches, feasible and infeasible regions were illustrated in the supplementary material (S5).

4.2. Different optimal management scenarios

In this subsection, we present the results of the three management scenarios. The approximated Pareto fronts achieved by the three management scenarios using the BO approach are presented in Fig. 6. It is worth mentioning that the number of attained optimal solutions for each management is different, which corresponds to the complexity of the optimization problem, the search on the rugged landscape, and the wideness of the decision variable space. The size of the non-dominated feasible solution set of management scenario 2 is the largest and in contrast, management scenario, 1 has few optimal solutions.

The results show that management scenario 2 (no regional abstractions) outperforms the other two management scenarios in terms of the total cost, which is expected because overexploitation is the main driver for SWI. Management scenario 3, which forced the remediation management to extract a minimum amount of brackish water within the intrusion wedge led to an increase in the total cost compared to unrestricted wells rates in management scenario 1. The obtained results endorse the robustness of the BO approach and prove its capabilities to capture the behavior of SWI under different management scenarios, handle the constraints, and provide optimal solutions.

Fig. 7 demonstrates the upper and lower bounds and the medians for the X coordinate, Y coordinate, and the total flow (Q^{inj}_{total}, Q^{abs}_{total}) for the injection and abstraction barriers obtained for each management scenario. The X-coordinate of the injection barriers (Fig. 7a), and the Y-coordinate of both injection and abstraction barriers, for all the management scenarios, showed no location prevalence, such that the solutions took on different values covering the whole range of the variable (Fig. 7b). On the other hand, the X-coordinate of the abstraction hydraulic barriers for the optimal solutions of management scenarios 1 and 3 were obtained close to the sea (Fig. 7a). This result agrees with the literature that the abstraction barriers should be placed near the sea for more effective remediation (Ebeling et al., 2019; Mahesha, 1996; Pool and Carrera, 2010). However, the results of management scenario 2 showed that the abstraction barriers can be located at different places covering roughly the whole design space (Fig. 7a & 7b). This indicates that the feasible region is large, which is the direct consequence of no abstractions.

The results of the total injection and abstraction rates showed that the injection has a greater influence on the efficiency of the mixed barrier remediation system than the abstraction (Fig. 7c). This is consistent with the findings of previous studies (Ebeling et al., 2019; Pool and Carrera, 2010; Shi et al., 2020).

The required total discharge and recharge rates of the barriers for management scenario 2 are fairly low; the medians are 20 and 564 m^3/hr respectively (Fig. 7c). Ceasing/reducing the abstraction is the most beneficial and cost-effective countermeasure to prevent further SWI.

Table 3
Comparison of BO and NSGA-II algorithms.

Point of comparison	BO	NSGA-II	Remarks
Total computational time (hours)	19.34	371	BO was run for 2×100 evaluations, while NSGA-II was for 4000 evaluations.
Average time per one iteration (min)	11.6	5.6	
HV	2.61×10^{18}	2.75×10^{18}	
GD	2.41×10^{8}	3.11×10^{8}	
Total salt mass objective range (tons)	46.2 to 212	22.4 to 205	
Average intrusion length of 50% objective range (m)	0 to 476	0 to 433	
Total cost objective range (£)	1879 to 7372	2187 to 7880	

4.3. Analysis of approximated Pareto optimal solution for management scenario 1

A solution from the approximated Pareto front by BO of management scenario 1 was randomly selected with objective function values = (79.4×10^9 g, 128.76 m, £4261.8) to evaluate the effectiveness of the optimized mixed hydraulic barriers remediation system to control SWI. Fig. 8 presents the concentration distribution at the bottom of the aquifer at the start and the end of the management period. The salinity concentration at the locations of regional pumping wells did not exceed the imposed concentration constraint. Significant repulsion for the toe interface took place after the implementation of the optimal remediation measure. The spatial distribution of the abstraction and injection hydraulic barriers is shown in Fig. 8. The injection barriers were placed within the saline wedge around the initial 50% isochlor with 85% of the total injected flow and the rest was injected inland away from the initial toe interface. The abstraction barrier was close to the sea. The velocity vectors emphasize the ability of the remediation system to shift back the hydraulic gradient towards the sea. The injection has a significant contribution to the management strategy. The rates of the hydraulic barriers are presented in Table 4.

Two indices were calculated to quantify the transient remediation progress, the 50% isochlor relative repulsion index (RI_{50}) and the relative total salt mass index (MI) (Ebeling et al., 2019). RI_{50} calculates the incurred transient repulsion due to the remediation measure relative to the natural intrusion. MI estimates the obtained reduction in the total salt mass relative to the natural total salt mass in the aquifer. These indices can take positive values up to 1 which means reaching the natural intrusion condition, while negative values indicate more deterioration in terms of saline water volume or further seawater encroachment and 0 refers to the initial condition just before the management starts. Their equations are expressed as.

$$RI_{50} = \frac{L_0 - L_t}{L_0 - L_n} \tag{11}$$

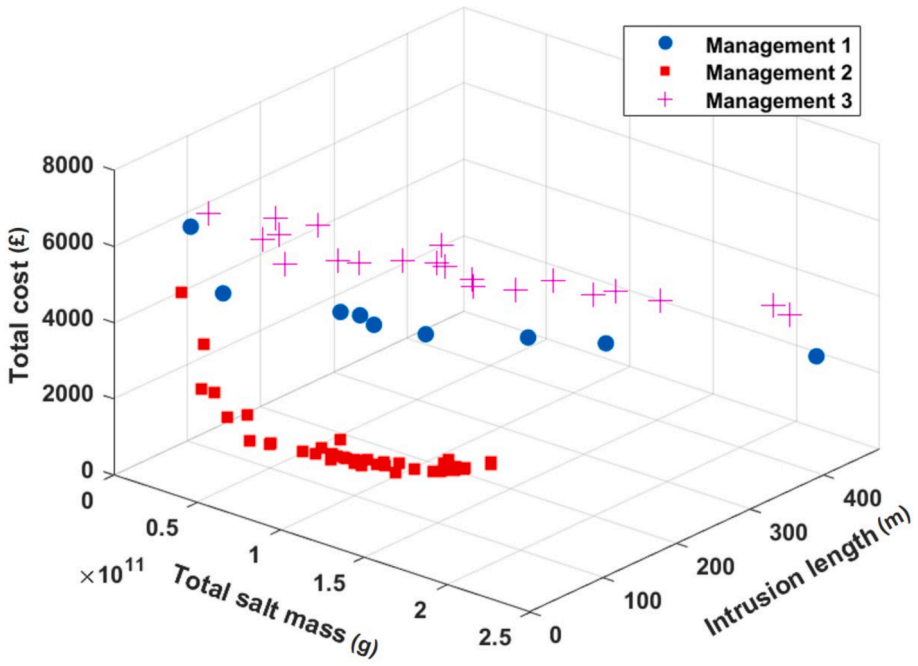

Fig. 6. Comparison between the objectives of the optimal solutions of management scenarios 1, 2, and 3 using BO approach.

$$MI = \frac{M_0 - M_t}{M_0 - M_n} \tag{12}$$

where L_0, M_0, L_t, M_t, L_n, M_n are the intrusion length and the total salt mass at the start of remediation, at time t from the start of remediation, and under the natural condition respectively. In the early stage, the water level increased in the aquifer due to the injected water. Part of the flow retreated the intrusion and the other part flowed inland diluting the saline water. However, there was still an inland lateral flow from the sea. This resulted in increasing the total salt mass within the aquifer until the overall flow turned towards the sea (Fig. 9). The mixed hydraulic barriers system precluded further SWI advances, pushed the saline wedge towards the sea, and succeeded to repel the intrusion to reach an average length that exceeded the natural intrusion condition by 21.3% of its length (Fig. 9). After approximately 1 year from the implementation of the management strategy, the system could generate a seaward hydraulic gradient, and by the end of the management period, the aquifer recovered from the salinization by 79.2% to achieve the natural condition.

The efficiency of the optimization is assessed by analyzing the adverse effect on the remediation measure of removing each barrier successively from the mixed hydraulic barriers system. This provides a measure of the contribution of each barrier to the improvement of the remediation. Table 4 illustrates the impact on the total salt mass, the intrusion length, and the maximum salinity at the regional pumping wells, caused by the omission of each barrier. BW2- injection barrier with the highest rate, had the strongest influence on SWI mitigation, while the BW6-abstraction barrier had the least effect.

The resulting evolution of the salinity at the hydraulic barriers due to the application of the remediation system and when the barrier is omitted is presented in Fig. 10. It can be seen from Fig. 10 and Table 4 that BW-1 is capable of reducing the aquifer salinity and pushing the seawater interface towards the coast, such that on its removal the salinity increased by 23%, and seawater invasion expanded by 24% (Fig. 10a). However, the quality of the used treated wastewater caused contamination to the aquifer, where its salinity is higher than the natural groundwater salinity.

The influence of each positive barrier corresponds to its rate; the higher the injection rate, the greater the improvement is, as shown for BW-2 (Fig. 10b), BW-3 (Fig. 10c), BW-4 (Fig. 10d), and BW-5 (Fig. 10e). The negative barrier BW-6 experienced a relatively sharp decline in the early stage of its operation (Fig. 10f). However after a short period, the salinity rose again, then it showed a similar decline trend in the salinity to that of the scenario of its removal from the remediation system with a slight decrease. The later rise in the salinity is due to the depression cone generated by the pumping, where at a certain point with further drawdown, It withdrew seawater causing more contamination. This phenomenon was also reported by Pool and Carrera (2010) in their study of using double negative barriers as a corrective measure to control SWI in low dynamic aquifers. The lateral seawater flux resulting from the drawdowns of the pumping wells reduces the system's efficiency at the late remediation stage. The positive barrier has a relatively small impact on the remediation improvement by less than 5% in terms of the salinity volume and impeding the intrusion. The assessment proved that the solution is efficiently optimized since deterioration was observed after discarding any of the barriers.

5. Discussion

Evolutionary algorithms and Bayesian optimization are two well-known research fields in optimization. They have a similar structure, including initialization, evaluation of the black-box function at a given sample point, and update to the current search seeking improvement in the next iteration. The process is repeated until reaching the termination criterion. The difference between them is in the update strategy to the search. NSGA-II (which belongs to evolutionary algorithms) uses a population-based search, that relies on crossover and mutation operators and diversity mechanisms to avoid getting trapped in local minima (Deb et al., 2002). This results in NSGA-II tending to need a huge number of evaluations to converge to the exact Pareto front. BO is based on learning from the previous samples and selecting the next samples by the optimization of the acquisition function (Jones et al., 1998). BO requires only a few expensive evaluations compared to NSGA-II (Yang et al., 2019a). This is due to its reliance on GPR and the acquisition function. GPR is a machine learning probabilistic model that replaces the high-fidelity simulation model, learns from previous evaluations about the relationship between the evaluation functions and the decision vectors, and allows fast evaluations of a great number of candidates within the

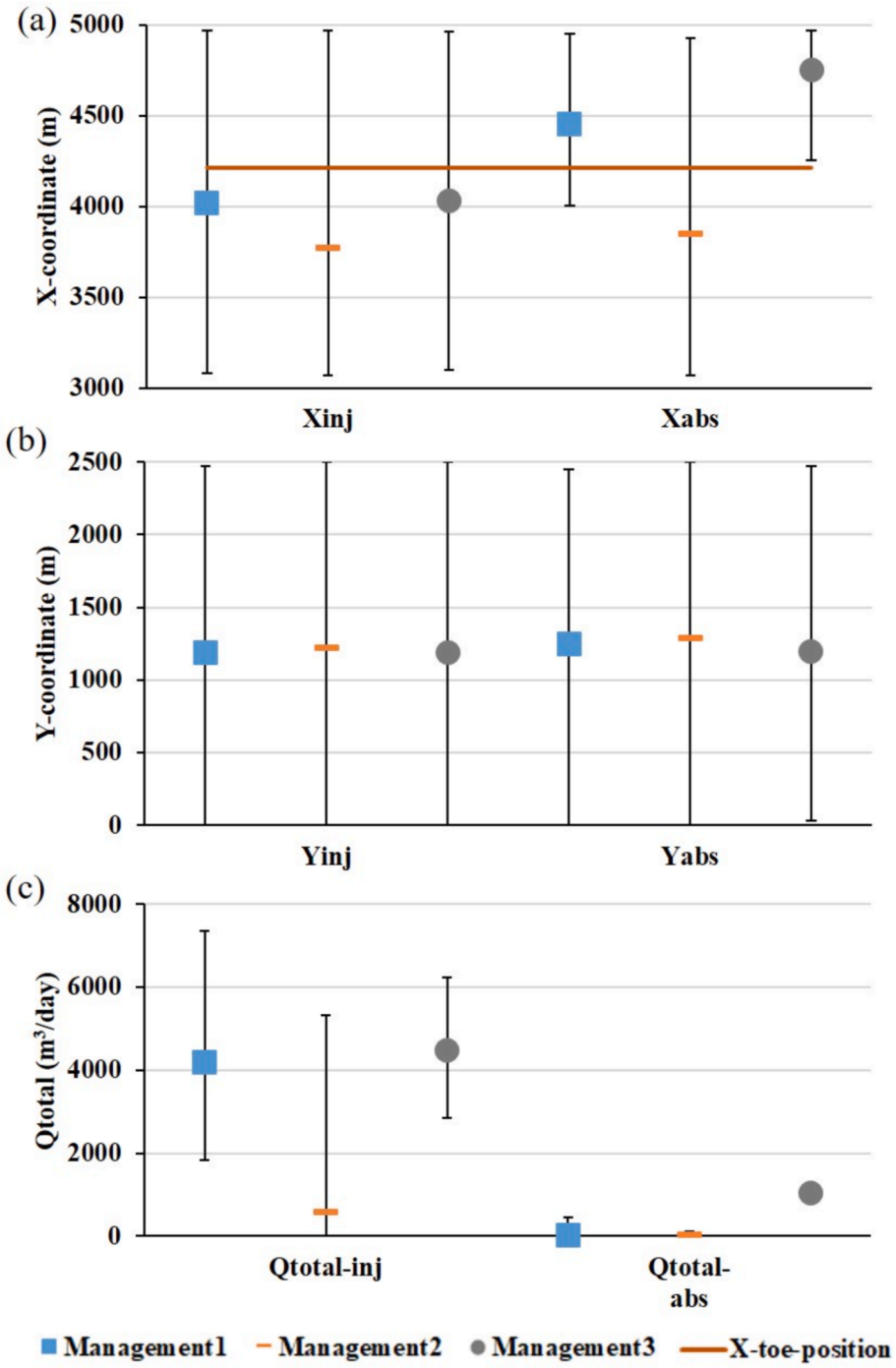

Fig. 7. Medians and variations in the variables for all management scenarios: a for X-coordinate, c for Y-coordinate, and d for the total injection and abstractions of hydraulic barriers.

optimization process of the acquisition function. The acquisition function uses the GPR models' evaluations and the associated uncertainty, to evaluate the performance improvement, and guides the choice of the next samples via its optimization. Therefore, it is suitable for optimizing SWI management problems that rely on computationally expensive functions. The HV and GD indicators (as performance indicators) showed the superiority of the BO compared to NSGA-II at the later stage of the search under a few evaluations (Fig. 5). Therefore, the main benefits of the BO approach are 1) accounting for the uncertainty in the predictions that offers a search efficient alternative through exploration (searching unexplored regions, where the prediction has high uncertainty) and exploitation (searching regions, where the prediction is minimum) when selecting the new promising sample (Shahriari et al., 2016) by the acquisition function, and 2) providing solutions on the approximated Pareto front with the least number of expensive evaluations.

Conversely, the consumed time for generating candidate solutions by BO is significantly higher than NSGA-II for each iteration (Table 3). Maximizing the acquisition function to generate candidate solutions is a time-consuming procedure (Daulton et al., 2020; Yang et al., 2019b). However, this time is relatively insignificant compared to the simulation time required for evaluating the expensive black-box functions. NSGA-II took a fixed amount of time, because it required less computation than BO per iteration.

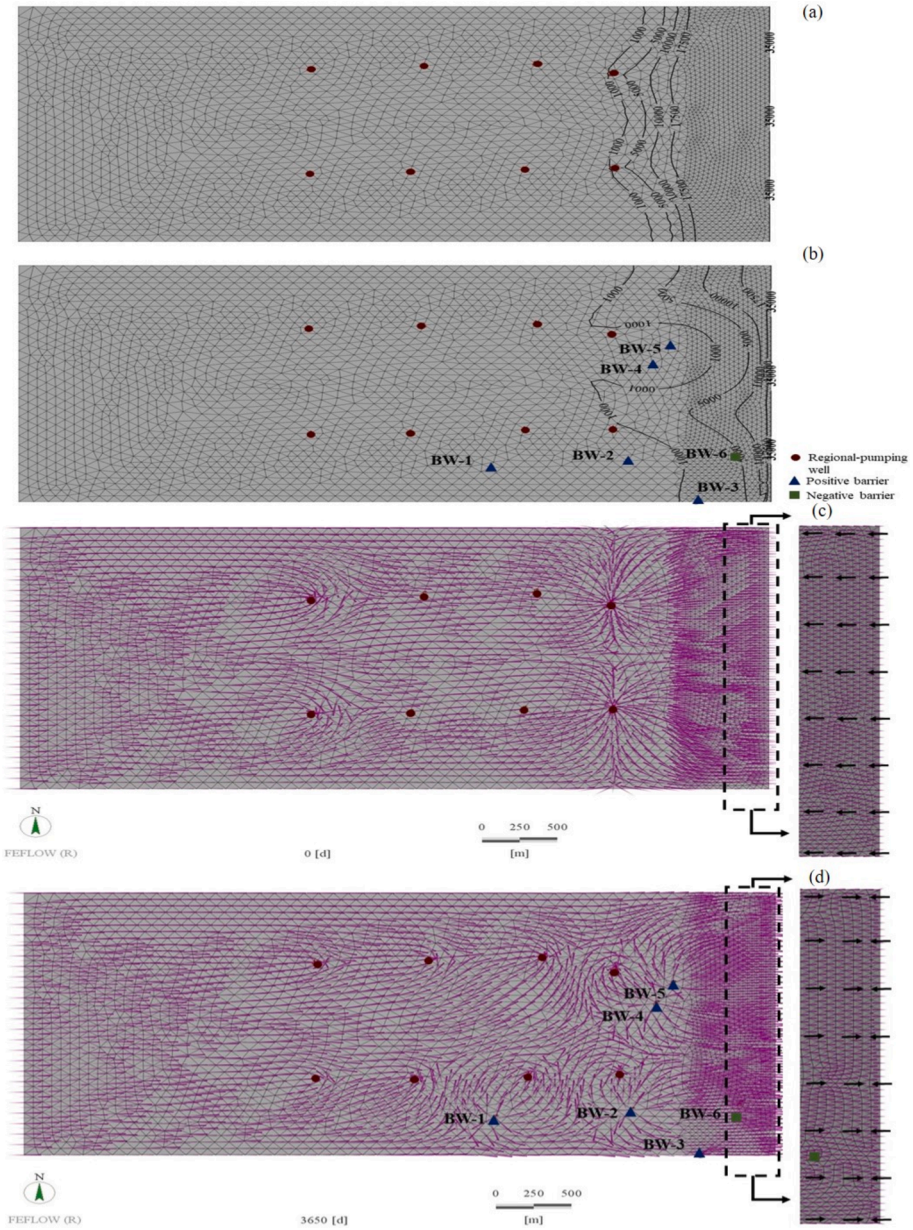

Fig. 8. Spatial distribution of the hydraulic barriers, salinity distribution at the aquifer bottom, and the velocity vectors at the aquifer bottom (a,c) before implementation of management strategy, (b,d) at the end of the management period.

Table 4
Average intrusion length, total mass salt in the aquifer, and the salinity concentration for each scenario.

Scenario	Avg_50% isochlor intrusion length (m)	Total mass salt (ton)	Salinity at Pumping well (mg/lit)	Omitted barrier rate (m^3/day)
Just before management	605.76	275.44	1466	–
Without management	912.49	372.46	12495.5	–
Optimal management	128.76	79.4	726.5	–
BW1-removal	159.91	98.0	1156.9	−644.1
BW2-removal	335.81	148	1955.1	−1484.7
BW3-removal	138.58	84.2	1111.7	−47.4
BW4-removal	275.80	134.5	1813.1	−1228.2
BW5-removal	231.24	116.7	1248.5	−845.5
BW6-removal	133.64	83.1	1107.5	+5.9

The drawback of the proposed algorithm is the pre-assignment for the required number of hydraulic barriers, i.e. the number of hydraulic barriers is not a decision variable. The traditional GP-based BO cannot be implemented when the optimization function is based on a variant number of decision vectors. However, SWI management problems often have the total cost as one of the objective functions, and it relies on the number of hydraulic barriers. Recently Chugh and Ymeraj (2022) proposed an extension to the applicability of multi-objective Bayesian optimization to overcome this limitation.

Based on the results of three different management scenarios, it was shown that there are no specific spatial configurations for wells and pumping/injection rates that can be provided as a one-solution fits all (Fig. 7). This agrees with the literature where, placing the abstraction hydraulic barriers seaside and the injection barriers inland e.g. (Shi et al., 2020) or vice versa e.g. (Ebeling et al., 2019) were both used for the injection-abstraction remediation system. A well-designed mixed barrier system taking into consideration the hydrogeological and geological aquifer conditions needs many combinations of the barrier

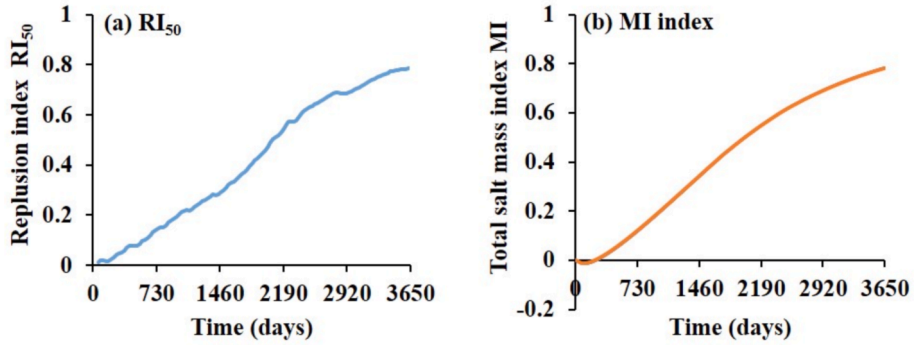

Fig. 9. Variations of transient repulsion (RI50) and total salt mass indices (MI) with time for the remediation system.

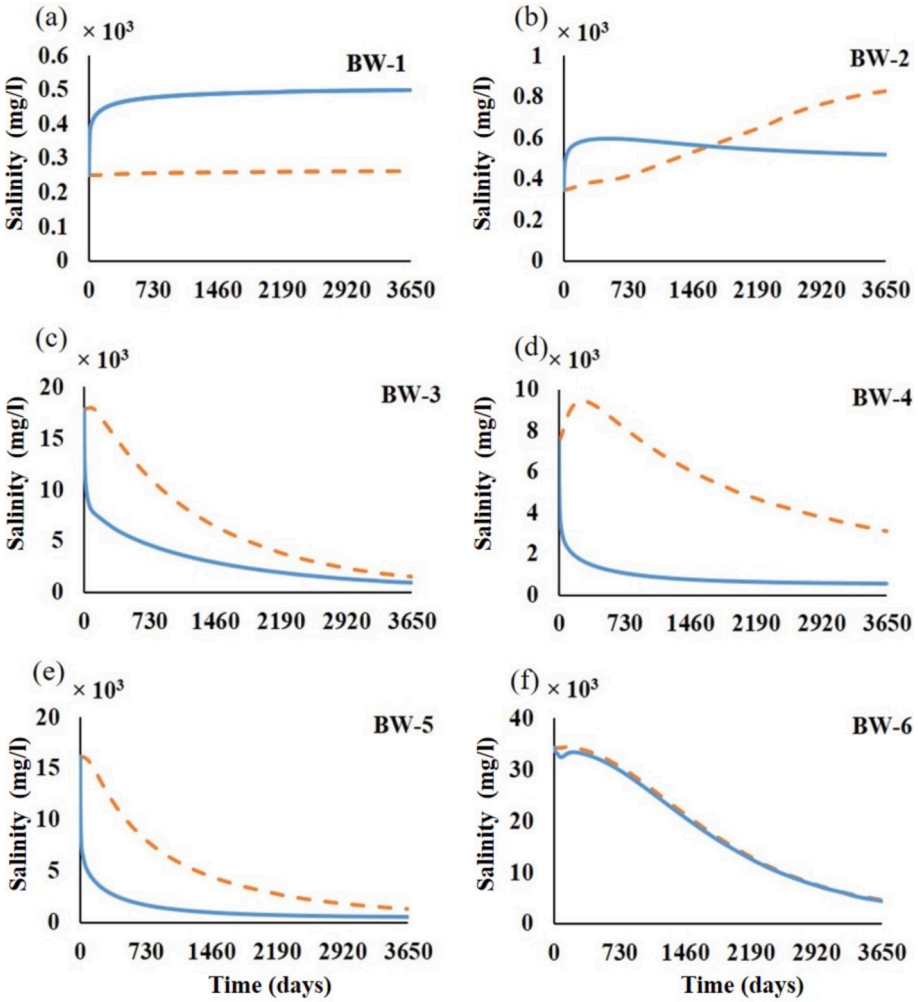

Fig. 10. Salinity concentration at the hydraulic barrier locations; solid line for the complete remediation system, dashed line for the omitted hydraulic barrier at this location, Y-axis represents the salinity concentrations in thousand mg/l against the time in days.

rates and locations to choose the best one among them. Consequently, it is necessary to identify an optimal management strategy, instead of testing limited combinations as has been done in previous studies.

6. Conclusions

This study evaluated the application of a constrained multi-objective Bayesian optimization approach to control seawater intrusion in a coastal aquifer. The approach was based on both GPR, as a surrogate model for each objective and constraint function, and qEHVI as an acquisition function to find the optimal well locations and rates for the mixed hydraulic barriers system to mitigate the SWI. The main conclusions that can be deduced from the results of the optimization approach are as follows:

1) The BO approach minimized the objective functions and satisfied the constraints with a limited number of simulations, providing a high-quality Pareto solution set, which is comparable to NSGA-II results under relatively unrestricted computational effort in terms of the hypervolume and the diversity of the Pareto solutions. Such

performance led to a 95% saving in the computational runtime. This proves its applicability to real-world coastal aquifer management problems, which involve computationally expensive variable-density groundwater models.

2) For a similar number of evaluations, BO is better in terms of data efficiency, where it has a higher rate of hypervolume improvement and/or lower generational distance, i.e., a better quality of the Pareto solutions. However, more computation time per evaluation is required. As a result, it is good to use evolutionary algorithms for problems where evaluating candidate solutions takes minimal time and BOs for more computationally expensive problems.
3) The optimal locations and rates for the abstraction and injection wells of mixed hydraulic barriers can take on different values within the entire design space. Efficient optimization can identify the best locations and rates, considering the aquifer characteristics.

The main findings from the implementation of different management scenarios for the design of the mixed hydraulic barriers are as follows:

1) The injection barriers offer higher control over the remediation measure in terms of the intrusion length and the total salt mass in the aquifer. The higher the injection rate, the greater the influence is on the SWI mitigation.
2) Attention should be paid to the quality of the injected water and the location of the injection. Recharging the aquifer with treated wastewater, which has a salinity that exceeds the salinity of natural groundwater would lead to the contamination of the freshwater, even though it may repel the SWI. A constraint needs to be imposed on the potential locations for the injection barriers in the proposed management to avoid the risk of local contamination.
3) The main advantage of the abstraction of brackish water is its role as an alternative freshwater resource, where the abstracted water can be desalinated at less cost than seawater.
4) The abstraction barriers seem to be more effective in the early stage of the implementation, rather than at a later stage when the generated depression cones may start to withdraw seawater causing saltwater to flow laterally inland and increase the salinity.

In summary, the Bayesian optimization approach proved to be a reliable and accurate approach for seawater intrusion control models and could be incorporated into the simulation–optimization framework of coastal management problems. Future research will focus on the application of the BO approach to real-world coastal management optimization problems.

CRediT authorship contribution statement

Samia Saad: Conceptualization, Methodology, Software, Formal analysis, Investigation, Validation, Resources, Visualization, Writing – original draft, Writing – review & editing, Funding acquisition. **Akbar A. Javadi:** Supervision, Conceptualization, Writing – review & editing. **Tinkle Chugh:** Methodology, Software, Validation, Visualization, Writing – review & editing. **Raziyeh Farmani:** Supervision, Writing – review & editing.

Declaration of Competing Interest

The authors declare that they have no known competing financial interests or personal relationships that could have appeared to influence the work reported in this paper.

Acknowledgments

The first author is funded by the Ministry of Higher Education of the Arab Republic of Egypt, Netwon Mosharafa scholarship [ID: NMM26/17]. The authors would like to express their gratitude to the DHI group for providing the free license of FEFLOW. We would like to take this opportunity to thank the three anonymous reviewers, the associate editor, and the editor for their valuable comments that have certainly improved the quality of the paper.

Appendix A. Supplementary data

Supplementary data to this article can be found online at https://doi.org/10.1016/j.jhydrol.2022.128021.

References

Asher, M.J., Croke, B.F.W., Jakeman, A.J., Peeters, L.J.M., 2015. A review of surrogate models and their application to groundwater modeling. Water Resour. Res. 51 (8), 5957–5973. https://doi.org/10.1002/2015WR016967.

Ayers, R.S., Westcot, D.W., Food Agriculture Organization of the United Nations, 1985. Water quality for agriculture. Food and Agriculture Organization of the United Nations, Rome.

Bachtouli, S., Comte, J.-C., 2019. Regional-scale analysis of the effect of managed aquifer recharge on saltwater intrusion in irrigated coastal aquifers: long-term groundwater observations and model simulations in NE Tunisia. J. Coastal Res. 35 (1), 91–109.

Balandat, M., et al., 2020. BoTorch: A framework for efficient Monte-Carlo Bayesian optimization. Advances in Neural Information Processing Systems (NeurIPS).

Boussinesq, J.V., 1903. Théorie analytique de la chaleur mise en harmonie avec la thermodynamique et avec la théorie mécanique de la lumière. Gauthier-Villars et C-ie, éditeurs, Paris.

Candelieri, A., Perego, R., Archetti, F., 2021. Green machine learning via augmented Gaussian processes and multi-information source optimization. Soft Computing, 25 (19): 12591-12603.

Christelis, V., Regis, R.G., Mantoglou, A., 2018. Surrogate-based pumping optimization of coastal aquifers under limited computational budgets. J. Hydroinf. 20 (1), 164–176.

Chugh, T., Ymeraj, E., 2022. Wind Farm Layout Optimisation using Set Based Multi-objective Bayesian Optimisation. arXiv preprint arXiv:2203.17065.

Daulton, S., Balandat, M., Bakshy, E., 2020. Differentiable expected hypervolume improvement for parallel multi-objective Bayesian optimization. arXiv preprint arXiv:2006.05078.

Deb, K., Pratap, A., Agarwal, S., Meyarivan, T., 2002. A fast and elitist multiobjective genetic algorithm: NSGA-II. IEEE Trans. Evol. Comput. 6 (2), 182–197. https://doi.org/10.1109/4235.996017.

Diersch, H.-J.-G., 1988. Finite element modelling of recirculating density-driven saltwater intrusion processes in groundwater. Adv. Water Resour. 11 (1), 25–43.

Diersch, H.-J.-G., 2013. FEFLOW: finite element modeling of flow, mass and heat transport in porous and fractured media. Springer Science & Business Media.

Ebeling, P., Händel, F., Walther, M., 2019. Potential of mixed hydraulic barriers to remediate seawater intrusion. Sci. Total Environ. 693, 133478 https://doi.org/10.1016/j.scitotenv.2019.07.284.

Emmerich, M.T.M., Deutz, A.H., Klinkenberg, J.W., 2011. Hypervolume-based expected improvement: Monotonicity properties and exact computation, 2011 IEEE Congress of Evolutionary Computation (CEC), pp. 2147-2154. DOI:10.1109/CEC.2011.5949880.

Emmerich, M.T.M., Giannakoglou, K.C., Naujoks, B., 2006. Single- and multiobjective evolutionary optimization assisted by Gaussian random field metamodels. IEEE Trans. Evol. Comput. 10 (4), 421–439. https://doi.org/10.1109/TEVC.2005.859463.

Fisher, R.A., 1992. Statistical methods for research workers, Breakthroughs in statistics. Springer, pp. 66-70.

Garrido-Merchán, E.C., Hernández-Lobato, D., 2020. Dealing with categorical and integer-valued variables in bayesian optimization with gaussian processes. Neurocomputing 380, 20–35.

Herrera-Franco, G., Carrión-Mero, P., Montalván-Burbano, N., Mora-Frank, C., Berrezueta, E., 2022. Bibliometric analysis of groundwater's life cycle assessment research. Water 14 (7), 1082.

Howard, K.W., 2015. Sustainable cities and the groundwater governance challenge. Environ. Earth Sci. 73 (6), 2543–2554.

Hupkens, I., Deutz, A., Yang, K., Emmerich, M., 2015. Faster exact algorithms for computing expected hypervolume improvement, international conference on evolutionary multi-criterion optimization. Springer, pp. 65-79.

Jones, D.R., Schonlau, M., Welch, W.J., 1998. Efficient global optimization of expensive black-box functions. J. Global Optim. 13 (4), 455.

Kopsiaftis, G., Protopapadakis, E., Voulodimos, A., Doulamis, N., Mantoglou, A., 2019. Gaussian process regression tuned by bayesian optimization for seawater intrusion prediction. Computational intelligence and neuroscience, 2019.

Krityakierne, T., Baowan, D., 2020. Aggregated GP-based Optimization for Contaminant Source Localization. Operations Research Perspectives, 7: 100151.

Lal, A., Datta, B., 2020. Performance evaluation of homogeneous and heterogeneous ensemble models for groundwater salinity predictions: a regional-scale comparison study. Water Air Soil Pollut. 231 (6), 320. https://doi.org/10.1007/s11270-020-04693-w.

Li, M., Yao, X., 2019. Quality evaluation of solution sets in multiobjective optimisation: a survey. ACM Comput. Surv. (CSUR) 52 (2), 1–38.

Liu, Y., Wei, J., Li, X., Li, M., 2019. Generational distance indicator-based evolutionary algorithm with an improved niching method for many-objective optimization problems. IEEE Access 7, 63881–63891.

Luo, C., Shimoyama, K., Obayashi, S., 2014. Kriging model based many-objective optimization with efficient calculation of expected hypervolume improvement, 2014 IEEE Congress on Evolutionary Computation (CEC). IEEE, pp. 1187-1194.

Mahesha, A., 1996. Control of Seawater Intrusion through Injection-Extraction Well System. J. Irrig. Drain. Eng. 122 (5), 314–317.

McKay, M.D., Beckman, R.J., Conover, W.J., 1979. A comparison of three methods for selecting values of input variables in the analysis of output from a computer code. Technometrics 21 (2), 239–245.

Metcalf, et al., 2014. Wastewater Engineering: Treatment and Resource Recovery. McGraw Hill Education.

Minasny, B., McBratney, A.B., 2006. A conditioned Latin hypercube method for sampling in the presence of ancillary information. CAGEO Comput. Geosci. 32 (9), 1378–1388.

O'Hagan, A., 2006. Bayesian analysis of computer code outputs: a tutorial. Reliab. Eng. Syst. Saf. 91 (10–11), 1290–1300.

Park, N., Shi, L., 2015. A comprehensive sharp-interface simulation-optimization model for fresh and saline groundwater management in coastal areas. Hydrogeol. J. 23 (6), 1195–1204. https://doi.org/10.1007/s10040-015-1268-8.

Pirot, G., Krityakierne, T., Ginsbourger, D., Renard, P., 2019. Contaminant source localization via Bayesian global optimization. Hydrol. Earth Syst. Sci. 23 (1), 351–369.

Pool, M., Carrera, J., 2010. Dynamics of negative hydraulic barriers to prevent seawater intrusion. Hydrogeol. J. 18 (1), 95–105. https://doi.org/10.1007/s10040-009-0516-1.

Pourmohamad, T., Lee, H.K.H., 2021. Bayesian Optimization Via Barrier Functions. J. Comput. Graph. Statist. 1–10 https://doi.org/10.1080/10618600.2021.1935270.

Rajabi, M.M., Ketabchi, H., 2017. Uncertainty-based simulation-optimization using Gaussian process emulation: application to coastal groundwater management. J. Hydrol. 555, 518–534. https://doi.org/10.1016/j.jhydrol.2017.10.041.

Rasmussen, C.E., Williams, C.K., 2006. Gaussian Processes for Machine Learning, 2. MIT press Cambridge, MA.

Razavi, S., Tolson, B.A., Burn, D.H., 2012. Review of surrogate modeling in water resources. Water Resour. Res. 48 (7).

Roy, D.K., Datta, B., 2020. Modelling and management of saltwater intrusion in a coastal aquifer system: a regional-scale study. Groundwater Sustain. Dev. 11, 100479 https://doi.org/10.1016/j.gsd.2020.100479.

Shahriari, B., Swersky, K., Wang, Z., Adams, R.P., Freitas, N.d., 2016. Taking the Human Out of the Loop: A Review of Bayesian Optimization. Proceedings of the IEEE, 104 (1): 148-175. DOI:10.1109/JPROC.2015.2494218.

Shi, L., Lu, C., Ye, Y., Xie, Y., Wu, J., 2020. Evaluation of the performance of multiple-well hydraulic barriers on enhancing groundwater extraction in a coastal aquifer. Adv. Water Resour. 144, 103704 https://doi.org/10.1016/j.advwatres.2020.103704.

Snoek, J., Larochelle, H., Adams, R.P., 2012. Practical bayesian optimization of machine learning algorithms. In: Advances in neural information processing systems, p. 25.

Song, J., et al., 2018. Adaptive surrogate model based multiobjective optimization for coastal aquifer management. J. Hydrol. 561, 98–111.

Van Ty, T., et al., 2021. Spatiotemporal variations in groundwater levels and the impact on land subsidence in CanTho, Vietnam. Groundwater for Sustain. Develop. 15, 100680.

Wang, C., et al., 2014. An evaluation of adaptive surrogate modeling based optimization with two benchmark problems. Environ. Modell. Software 60, 167–179. https://doi.org/10.1016/j.envsoft.2014.05.026.

World Health Organization, 2004. Guidelines for drinking-water quality, 1. World Health Organization (WHO).

Yang, K., Emmerich, M., Deutz, A., Bäck, T., 2019a. Efficient computation of expected hypervolume improvement using box decomposition algorithms. J. Global Optim. 75 (1), 3–34. https://doi.org/10.1007/s10898-019-00798-7.

Yang, K., Emmerich, M., Deutz, A., Bäck, T., 2019b. Multi-objective Bayesian global optimization using expected hypervolume improvement gradient. Swarm Evol. Comput. 44, 945–956.

Zitzler, E., Brockhoff, D., Thiele, L., 2007. The hypervolume indicator revisited: On the design of Pareto-compliant indicators via weighted integration, International Conference on Evolutionary Multi-Criterion Optimization. Springer, pp. 862-876.